Hamiltonian Engineering with Multicolor Drives for Fast Entangling Gates and Quantum Crosstalk Cancellation

K. X. Wei, E. Magesan, I. Lauer, S. Srinivasan, D. F. Bogorin, S. Carnevale, G. A. Keefe, Y. Kim, D. Klaus, W. Landers, N. Sundaresan, C. Wang, E. J. Zhang, M. Steffen, O. E. Dial, D. C. McKay, and A. Kandala

Phys. Rev. Lett. **129**, 060501 — Published 4 August 2022

DOI: 10.1103/PhysRevLett.129.060501

Hamiltonian engineering with multi-color drives for fast entangling gates and quantum crosstalk cancellation

K. X. Wei,* E. Magesan, I. Lauer, S. Srinivasan, D. F. Bogorin, S. Carnevale, G. A. Keefe, Y. Kim, D. Klaus, W. Landers, N. Sundaresan, C. Wang, E. J. Zhang, M. Steffen, O. E. Dial, D. C. McKay,† and A. Kandala‡
IBM Quantum, IBM T.J. Watson Research Center, Yorktown Heights, NY 10598, USA
(Dated: June 29, 2022)

Quantum computers built with superconducting artificial atoms already stretch the limits of their classical counterparts. While the lowest energy states of these artificial atoms serve as the qubit basis, the higher levels are responsible for both a host of attractive gate schemes as well as generating undesired interactions. In particular, when coupling these atoms to generate entanglement, the higher levels cause shifts in the computational levels that leads to unwanted ZZ quantum crosstalk. Here, we present a novel technique to manipulate the energy levels and mitigate this crosstalk with simultaneous off-resonant drives on coupled qubits. This breaks a fundamental deadlock between qubit-qubit coupling and crosstalk. In a fixed-frequency transmon architecture with strong coupling and crosstalk cancellation, additional cross-resonance drives enable a 90 ns CNOT with a gate error of (0.19 ± 0.02) %, while a second set of off-resonant drives enable a novel CZ gate. Furthermore, we show a definitive improvement in circuit performance with crosstalk cancellation over seven qubits, demonstrating the scalability of the technique. This work paves the way for superconducting hardware with faster gates and greatly improved multi-qubit circuit fidelities.

Existing quantum processors [1, 2] based on superconducting transmon qubits are pushing the limits of classical simulability. However, the realization of quantum advantage requires these processors to scale up in both size and operational fidelity. Reaching a suitable threshold on both counts would further enable the realization of a fault tolerant quantum computer. These objectives require overcoming several technical challenges, notably, two-qubit gate fidelity, crosstalk, system stability and qubit coherence. One common architecture, based on fixed-frequency transmon qubits with fixed couplings, has a distinct advantage in terms of stability and coherence, but has limitations on gate speed and minimizing crosstalk due to always on interactions, and their relation to the exchange coupling strength, J. While a larger J enables a faster entangling gate, the coupling leads to state dependent frequency shifts of neighboring coupled qubits, which is a source of quantum crosstalk that takes the form of a ZZ interaction in the system Hamiltonian. This is formally seen from the standard cQED Hamiltonian for a pair of coupled transmons ($i = \{0, 1\}$), modelled as Duffing oscillators,

$$H_0/h = \sum_{i=\{0,1\}} \left(\nu_i \hat{a}_i^\dagger \hat{a}_i + \frac{\alpha_i}{2} \hat{a}_i^\dagger \hat{a}_i \left(\hat{a}_i^\dagger \hat{a}_i - 1\right)\right) + J(\hat{a}_0^\dagger + \hat{a}_0)(\hat{a}_1^\dagger + \hat{a}_1), \quad (1)$$

with bare qubit frequencies ν_i, bare anharmonicities α_i and coupling strength J. The coupling dresses the energy levels, and the crosstalk arising from state dependent frequency shifts is expressed as,

$$\nu_{ZZ} = (\nu_{11} - \nu_{10}) - (\nu_{01} - \nu_{00}). \quad (2)$$

For fixed couplings, this is an always-on source of crosstalk, referred to as a static ZZ interaction, with the following perturbative form,

$$\nu_{ZZ,s} = -\frac{2J^2(\alpha_0 + \alpha_1)}{(\alpha_1 - \Delta_{0,1})(\alpha_0 + \Delta_{0,1})}, \quad (3)$$

where $\Delta_{0,1}$ represents the qubit-qubit detuning. This crosstalk has been seen to be an important limitation to multi-qubit circuit performance in tests of quantum volume [3], randomized benchmarking [4], and error correction codes [5], and may prevent device scaling [6]. Several hardware strategies have been employed to mitigate this crosstalk. The simplest approach, as seen from Eq. (3), is to lower J, however, this comes at the expense of gate speed and lowers the overall gate fidelity due to finite qubit coherence. More involved strategies include the the introduction of tunable J coupling [2, 7, 8]; coupling different flavors of qubits with opposite signs of anharmonicity [9–11] (see Eq. (3)); and the use of engineered multi-path coupling elements [11–15]. An alternative approach employs the AC Stark effect, using off-resonant radiation to selectively tune the energy levels, and modulate ZZ, as seen from Eq. (2). This has been demonstrated with a single near-resonant, continuous wave (CW) drive in flux-tunable superconducting qubit architectures [16, 17]. However, this requires being close to a resonant transition outside the computational space, and is susceptible to charge noise in transmon qubits.

In this work we show that the ZZ interaction for a pair of coupled transmon qubits can be tuned over several orders of magnitude by far-off resonant driving on *both* qubits, an effect that we designate siZZle

- Stark induced ZZ by level excursions. To describe the physics of siZZle, we consider the Hamiltonian of Eqn. (1) and add off-resonant drives on both qubits,

$$H_{\text{siZZle}}/h = H_0/h + \sum_{i=\{0,1\}} \Omega_i \cos(2\pi\nu_d t + \phi_i)(\hat{a}_i^\dagger + \hat{a}_i), \quad (4)$$

with amplitudes Ω_i, phases ϕ_i, and a common frequency ν_d . The device schematic in Fig. 1(a) depicts a simple direct capacitive coupling between the qubits that produces the Hamiltonian model of Eq. 4. In the limit of $\Omega_i/|\nu_d - \nu_i| \ll 1$, we can write the dressed RWA Hamiltonian as,

$$H_{\text{eff}}/h = \tilde{\nu}_{ZI} ZI/4 + \tilde{\nu}_{IZ} IZ/4 + \tilde{\nu}_{ZZ} ZZ/4, \quad (5)$$

where the tilde notation refers to being in the doubly-dressed frame with respect to the exchange coupling and Stark tones. To second order in Ω_i and first order in J, the ZZ coefficient is,

$$\tilde{\nu}_{ZZ} = \nu_{ZZ,s} + \frac{2J\alpha_0\alpha_1\Omega_0\Omega_1\cos(\phi_0 - \phi_1)}{\Delta_{0,d}\Delta_{1,d}(\Delta_{0,d}+\alpha_0)(\Delta_{1,d}+\alpha_1)}, \quad (6)$$

where the static term is given by Eqn. (3). In the above equations, $\Delta_{i,j} = (\nu_i - \nu_j)$ denotes detunings where $i, j \in \{0, 1, d\}$. The most significant contribution to the Stark shifts comes from the term associated with a single, isolated drive

$$\tilde{\nu}_{ZI,\text{single}} = -\frac{\Omega_0^2\alpha_0}{\Delta_{0,d}(\Delta_{0,d}+\alpha_0)}, \quad (7)$$

which will be of significance in later discussions for the impact of the Stark tones on qubit coherence. A formal derivation of these expressions is discussed in the Supplementary Information. Eq. (6) reveals the various control knobs to manipulate the strength of the Stark induced ZZ interaction: the amplitudes of the two tones, the drive-qubit detunings, the anharmonicities, and the phase differences between the two drive tones.

Fig. 1 discusses the physics of siZZle, employing the parameters of the primary two-qubit device studied in this work, device A. The parameters are given in Table I. We perform numerical diagonalization of Eq. (4) after moving into the frame of the drive. We see good agreement between the numerical calculations and the experimentally measured ZZ values. Figure 1 also reveal two interesting regimes of operation. At fairly modest drives, we observe see that we can cancel the ZZ interaction to operate at $\tilde{\nu}_{ZZ} \sim 0$. At stronger drive amplitudes, one can generate large ZZ rates for two qubit entangling gates.

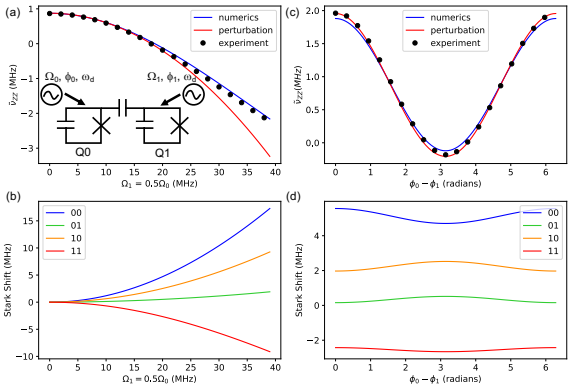

FIG. 1. (a) Modulation of the ZZ interaction strength $\tilde{\nu}_{ZZ}$ as the Rabi amplitude of the Stark tones is swept (ratio $\Omega_1/\Omega_0 = 0.5$) for fixed frequency $\nu_d = 5.075$ GHz and phase difference $\phi = \pi$. The inset shows a circuit representation of the primary two-qubit device discussed in this work. (b) The corresponding excursions of the computational levels, calculated numerically, to generate the $\tilde{\nu}_{ZZ}$ shown in (a).(c) Modulation of the ZZ interaction strength $\tilde{\nu}_{ZZ}$ as the phase difference between the Stark tones is swept, for fixed frequency $\nu_d = 5.075$ GHz and and drive amplitudes $\Omega_1 = 0.5\Omega_0 = 20$ MHz. Experimental data (black circles) is compared to numerical (blue line) and perturbative (red line) calculations using the device parameters of Table 1 in (a) and (c). (d) The corresponding excursions of the computational levels, calculated numerically, to generate the $\tilde{\nu}_{ZZ}$ shown in (c).

	$\tilde{\nu}_0$	$\tilde{\nu}_1$	$\tilde{\alpha}_0$	$\tilde{\alpha}_1$
No siZZle	4.960	5.016	-0.283	-0.287
siZZle	4.953	5.014	-0.276	-0.286

TABLE I. Qubit frequencies for device A depicted in Fig. 1(a) before and after ZZ cancellation. All the numbers are in units of GHz. We note that these numbers represent the experimentally measured frequencies, dressed by the coupling $J = 7.745$ MHz.

These regimes of operation are discussed in Fig. 2 and 3.

In the first regime of operation, siZZle is used to cancel ZZ, which can be utilized to increase the speed of entangling gates, such as cross-resonance (CR) [18, 19], which are set by the coupling strength J. As discussed previously in Eq. 3, increasing J typically leads to large values of static ZZ crosstalk. Recent work [14] with multi-path couplers demonstrated a way to break the standard relationship between J and $\nu_{ZZ,\text{static}}$ (operating at $J/\nu_{ZZ,\text{static}} \sim 130$), leading to state-of-the art CR gate fidelities. A drawback of the multi-path coupler approach is that $\nu_{ZZ,\text{static}}$ depends strongly on the qubit fre-

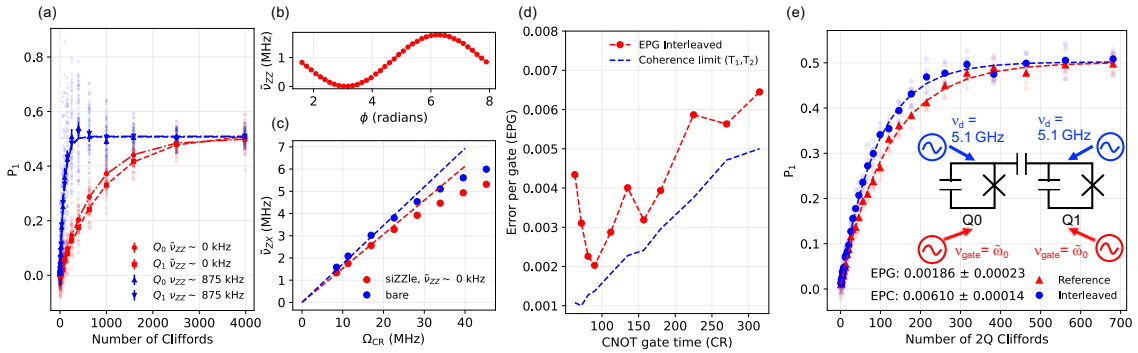

FIG. 2. (a) Simultaneous randomized benchmarking (RB) of 50 ns single qubit gates in the absence of static ZZ cancellation (blue) leads to an average EPG of 6.6e-3. After static ZZ cancellation with a pair of CW Stark tones at $\nu_d = 5.1$ GHz, the EPG dramatically improves to 7.1e-4 (red). Bold symbols represent mean of the individual seeds (represented by light symbols), and dotted lines are exponential fits to the decay of the excited state probability P_1. (b) Phase calibration of the CW Stark tones to $\tilde{\nu}_{ZZ} \sim 0$. (c) Strength of ZX interaction $\tilde{\nu}_{ZX}$ versus cross-resonance drive amplitude Ω_{CR} with (red) and without (blue) static ZZ cancellation. Here, Q1 is the control qubit and Q0 is the target qubit. Bold circles represent experimentally measured rates, using Hamiltonian tomography. Dotted lines are perturbative estimates, see Supplemental Information. (d) EPG measured by interleaved RB, for direct CNOT gates constructed from cross-resonance, after ZZ cancellation, as a function of CNOT gate time. The blue dotted line represent the coherence limit to gate error from estimated using standard T_1 and T_2 measurements before every RB run. (e) Post-ZZ cancellation interleaved RB of a 90 ns direct CNOT gate reveals a best EPG of 1.86e-3, with an EPG upper bound of 4.0e-3.

quencies, and full ZZ cancellation is non-trivial in fixed frequency architectures given current precision over qubit frequency allocation [1]. Our quantum control approach to ZZ cancellation introduced here enables tuning to $\tilde{\nu}_{ZZ} \sim 0$ over a range of parameters since we have several degrees of freedom in our control space. Importantly, this allows for a decoupling of J and $\tilde{\nu}_{ZZ}$ so that fast, high-fidelity entangling gates are possible with minimal static crosstalk in an architecture consisting of standard single path couplers and nominally fixed-frequency qubits.

To test this, device A has a large coupling strength of $J \sim 7.745$ MHz, leading to a very large static ZZ interaction of $\nu_{ZZ,\mathrm{static}} = 875$ kHz. Without any further mitigation of ZZ, this prevents high-fidelity simultaneous single qubit operation due to strongly state-dependent qubit frequencies. This is seen in the decay and variance of simultaneous single qubit randomized benchmarking sequences shown in Fig. 2(a) with an estimated average error per gate (EPG) of 6.6e-3. In order to mitigate this crosstalk, we add continuous wave (CW) Stark drives to cancel ZZ and operate in a basis dressed by these off-resonant drives. The large choice of operating parameters for the ZZ cancellation tones makes identifying an optimal set of working parameters a complex task. First, we limit leakage out of the computational subspace by placing the ZZ cancellation tone above both qubits. Next, we optimize the detuning of the cancellation tone. Smaller detuning reduces the drive amplitude required for ZZ cancellation. There is a practical limit to the amount of amplitude that can delivered to the qubits before there is heating of system components. However, if the detuning is too small then the cancellation tone may start to interfere with the gate drive and time-dependent terms in the effective Hamiltonian in the frame of the drive can no longer be ignored.

For these reasons, we select $\nu_d = 5.1$ GHz, for device A. The CW amplitudes are chosen to be sufficient to just approach $\tilde{\nu}_{ZZ} \sim 0$ after phase calibration (i.e at $\phi = \pi$), see Fig. 2(b). We estimate the CW amplitudes from the independent qubit Stark shifts to be $\Omega_0 = 59$ MHz and $\Omega_1 = 22$ MHz. After tuning to $\tilde{\nu}_{ZZ} \sim 0$, the single qubit gates are recalibrated with the cancellation drives on. Reducing the ZZ in this way results in remarkable improvements in simultaneous single qubit operation for 50 ns gates, with an estimated EPG of 7.1e-4 from randomized benchmarking, see Fig. 2(a). We note that there are several operating points for achieving $\nu_{ZZ} \sim 0$, but operating at stronger CW amplitudes with larger Stark shifts can to lead to additional dephasing.

With ZZ cancelled and single-qubit gates calibrated, we now calibrate a two-qubit gate with cross-resonance. This entails additional drives on the control qubit (Q1) at the dressed target qubit (Q0) fre-

quency. In Fig. 2c, we measure the generated ZX rates versus CR drive amplitude from tomography of the CR drive Hamiltonian, with and without ZZ cancellation. The ZX rate is modified due to the presence of the cancellation tones, and the experimental data shows good agreement with a perturbative model for the ZX rate (see Supplementary material). However, as a consequence of the large J coupling, one can access fairly large ZX rates at modest CR drive amplitudes.

The large J coupling is also of consequence for the reduced control qubit Stark shift, discussed previously in [14], and the resulting stability of unechoed *direct* CNOT gates constructed using CR. We construct and calibrate direct CNOT gates, similar to [14], and study the gate error obtained from interleaved RB as a function of CNOT gate time in Fig. 2d. The calibration sequences and pulse shapes are detailed in the supplement. At the optimal gate time of 90 ns, we depict results from interleaved RB sequences in Fig. 2e, that we use to estimate an EPG of 1.86e-3, with an error per Clifford (EPC) of 6.0e-3 from standard RB. Our decomposition has 1.5 CNOT gates per Clifford and 2.56 non-Z single qubit gates per Clifford on average and this places a worst case upper bound on the EPG of EPC/1.5 $\sim$ 4.0e-3. However, we express confidence that the bounds are in practice a lot tighter, based on the ratio of EPG/EPC (see the analysis in [20]) and bootstrapped simulations discussed in the supplement. We also note that our gate errors fluctuate with changes in coherence and the defect environment [21] in the vicinity of the qubit frequencies. At the time of the displayed benchmarking, our measured coherence times for Q0(Q1) were $T_1 = 66$ (66) μs and $T_2 = 49(84)$ μs.

In the second regime of operation, siZZle can be used as a standalone method for performing a two-qubit gate due to the large ZZ rates that can be generated as shown in Figs. 1 In order to mitigate the static ZZ, we continue to use CW tones at $\nu_d =$ 5.1 GHz, but, additionally pulse a second set of off-resonant tones at a different frequency ν_{gate} to generate large $\tilde{\nu}_{ZZ}$. This is shown in Figure 3a, where we sweep the pulsed tone frequency and amplitudes ($\Omega_{0,\text{gate}} = \Omega_{1,\text{gate}}$) to generate $\tilde{\nu}_{ZZ}$ exceeding a few MHz. We provide a proof-of-concept example of siZZle gate operation at $\nu_{\text{gate}} = 4.9$ GHz, with maximum amplitudes $\Omega_{0,\text{gate}}, \Omega_{1,\text{gate}} \sim 26$ MHz. We calibrate the phase difference between the phase tones for maximum $\tilde{\nu}_{ZZ}$, and employ frame changes on the control and target qubits to construct a novel *direct* CZ gate of length 200 ns. Interleaved RB, shown in Fig. 3b reveals an EPG of 5e-3, with an EPG upper bound of 7.6e-3.

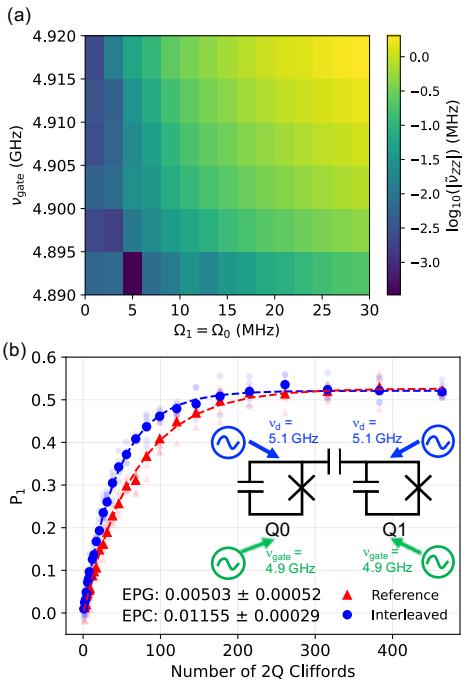

FIG. 3. (a) Post ZZ cancellation 2D sweep of ν_{ZZ} with pulsed Stark frequency ν_{gate} and amplitude, with the ratio of the two amplitudes fixed to $\Omega_0 = \Omega_1$, and phase calibrated to maximum contrast. The CW tones to cancel ZZ use the same parameters discussed in Fig 2, with $\nu_d = 5.1$ GHz. (b) Interleaved RB of a calibrated CZ gate based on siZZle reveals an EPG of 5e-3, with an EPG upper bound of 7.6e-3.

Finally, we study the impact of siZZle on multi-qubit circuit fidelity, using a line of 7 qubits from a 27 qubit device with a heavy-hex architecture [3], that we shall refer to as Device B. The device properties are detailed in the Supplementary Information. For the considered line of qubits, we choose a common Stark frequency set to 5.1 GHz, above all the qubit frequencies, leaving the individual amplitudes and phases as the free control parameters. For chosen amplitudes, we can operate the device at varying $\tilde{\nu}_{ZZ}$ levels merely by adjusting the pairwise phase difference, and re-calibrating the single and two qubit gates at the new dressed frequencies. We then use cross-resonance to calibrate an echo CNOT with rotary target drives, as in [22]. No large changes are observed in the CNOT gate fidelities, at the different $\tilde{\nu}_{ZZ}$ levels, which highlights the need for circuit-level benchmarks such as quantum volume (QV) [23] that are sensitive to accumulated ZZ errors from qubit idle times. In order to benchmark multi-qubit performance, we employ seven-qubit QV

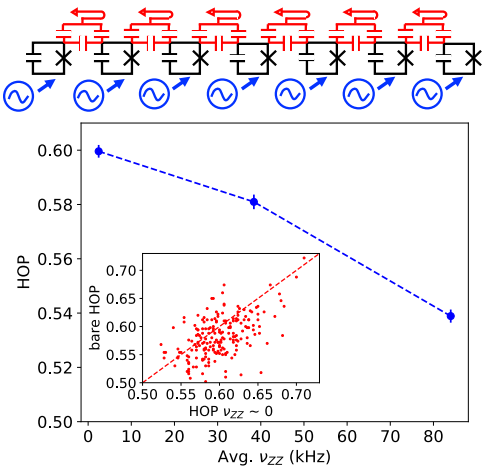

FIG. 4. (Top) A device schematic of the line of 7 qubits, with a combination of hardware and control approaches to ZZ modulation. The device employs multi-path couplers composed of a direct capacitive coupling and a $\lambda/4$ bus resonator. (Bottom) Average heavy output probability (HOP) for the same set of 200 random quantum volume (QV) circuits, at different levels of $\tilde{\nu}_{ZZ}$. We observe an improvement in HOP from 0.5810 ± 0.0027 to 0.5996 ± 0.0023 as the average $\tilde{\nu}_{ZZ}$ is tuned from the bare value ∼ 40 kHz to ∼ 0 kHz. Error bars represent standard error of the mean. The maximum and minimum $\tilde{\nu}_{ZZ}$ data points are tuned by setting the pair wise phase difference between the siZZle tones to $\phi \sim 0$ and $\phi \sim \pi$ respectively. The middle data point is measured in the absence of siZZle. (Inset) Scatter of individual circuit HOPs for the native (bare) device versus post-ZZ cancellation.

circuits and observe a systematic improvement in the heavy output probability (HOP) as $\tilde{\nu}_{ZZ}$ is suppressed. This highlights why ZZ cancellation will be crucial for improving the performance of superconducting quantum processors. The technique also opens up the path to more targeted studies of the impact of the ZZ interaction on spectator interactions and parallel gate operation, all in a single device.

In conclusion, we demonstrate an all microwave technique - siZZle - for arbitrary control of the ZZ interaction rate in coupled transmon devices. We use siZZle to demonstrate a novel high-fidelity CZ gate that could enable hardware-efficient implementations of near-term algorithms on existing fixed-frequency quantum processors. Furthermore, static ZZ cancellation with siZZle enables us to take cross-resonance past the 100 ns milestone for two-qubit gate time, with state-of-the-art fidelity. Finally, combining siZZle with hardware approaches to ZZ cancellation is leveraged to definitively improve multi-qubit circuit fidelity, and highlights the scalability of our technique. These results reveal quantum control with multi-color drive tones to be an attractive approach to extend the reach of fixed frequency superconducting quantum architectures.

We note recent independent work [24] reporting siZZle and a CZ gate based on the effect. Our current work includes Supplementary Information that details the theory of the siZZle effect, experimental sweeps of the parameter space, gate calibration, the effect of multi-path ZZ cancellation couplers, device details and effect on coherence, and simulations of interleaved randomized benchmarking with references [14, 20, 25–29]

Acknowledgements We thank M. Carroll, A. Corcoles, P. Gumann, M. Gordon, S. Hall, S. Hart, M. Kumph, J. Rozen, M. Takita for experimental contributions and D. McClure, P. Jurcevic for helpful discussions. The device bring-up, gate calibration and characterization work was supported by IARPA under LogiQ (contract W911NF-16-1-0114).

* xkwei@ibm.com
† dcmckay@us.ibm.com
‡ akandala@us.ibm.com

[1] E. J. Zhang, S. Srinivasan, N. Sundaresan, D. F. Bogorin, Y. Martin, J. B. Hertzberg, J. Timmerwilke, E. J. Pritchett, J.-B. Yau, C. Wang, et al., arXiv preprint arXiv:2012.08475 (2020).
[2] F. Arute, K. Arya, R. Babbush, D. Bacon, J. C. Bardin, R. Barends, R. Biswas, S. Boixo, F. G. Brandao, D. A. Buell, et al., Nature **574**, 505 (2019).
[3] P. Jurcevic, A. Javadi-Abhari, L. S. Bishop, I. Lauer, D. F. Bogorin, M. Brink, L. Capelluto, O. Günlük, T. Itoko, N. Kanazawa, et al., Quantum Science and Technology **6**, 025020 (2021).
[4] D. C. McKay, S. Sheldon, J. A. Smolin, J. M. Chow, and J. M. Gambetta, Phys. Rev. Lett. **122**, 200502 (2019).
[5] M. Takita, A. D. Córcoles, E. Magesan, B. Abdo, M. Brink, A. Cross, J. M. Chow, and J. M. Gambetta, Phys. Rev. Lett. **117**, 210505 (2016).
[6] C. Berke, E. Varvelis, S. Trebst, A. Altland, and D. P. DiVincenzo, arXiv preprint arXiv:2012.05923 (2020).
[7] Y. Chen, C. Neill, P. Roushan, N. Leung, M. Fang, R. Barends, J. Kelly, B. Campbell, Z. Chen, B. Chiaro, A. Dunsworth, E. Jeffrey, A. Megrant, J. Y. Mutus, P. J. J. O'Malley, C. M. Quintana, D. Sank, A. Vainsencher, J. Wenner, T. C. White, M. R. Geller, A. N. Cleland, and J. M. Martinis, Phys. Rev. Lett. **113**, 220502 (2014).
[8] J. Stehlik, D. M. Zajac, D. L. Underwood, T. Phung, J. Blair, S. Carnevale, D. Klaus, G. A. Keefe, A. Carniol, M. Kumph, M. Steffen, and O. E. Dial, Phys. Rev. Lett. **127**, 080505 (2021).

[9] P. Zhao, P. Xu, D. Lan, J. Chu, X. Tan, H. Yu, and Y. Yu, Phys. Rev. Lett. **125**, 200503 (2020).

[10] J. Ku, X. Xu, M. Brink, D. C. McKay, J. B. Hertzberg, M. H. Ansari, and B. L. T. Plourde, Phys. Rev. Lett. **125**, 200504 (2020).

[11] X. Xu and M. Ansari, Phys. Rev. Applied **15**, 064074 (2021).

[12] P. Mundada, G. Zhang, T. Hazard, and A. Houck, Physical Review Applied **12**, 054023 (2019).

[13] F. Yan, P. Krantz, Y. Sung, M. Kjaergaard, D. L. Campbell, T. P. Orlando, S. Gustavsson, and W. D. Oliver, Physical Review Applied **10**, 054062 (2018).

[14] A. Kandala, K. X. Wei, S. Srinivasan, E. Magesan, S. Carnevale, G. A. Keefe, D. Klaus, O. Dial, and D. C. McKay, Phys. Rev. Lett. **127**, 130501 (2021).

[15] P. Zhao, D. Lan, P. Xu, G. Xue, M. Blank, X. Tan, H. Yu, and Y. Yu, Phys. Rev. Applied **16**, 024037 (2021).

[16] A. Noguchi, A. Osada, S. Masuda, S. Kono, K. Heya, S. P. Wolski, H. Takahashi, T. Sugiyama, D. Lachance-Quirion, and Y. Nakamura, Phys. Rev. A **102**, 062408 (2020).

[17] H. Xiong, Q. Ficheux, A. Somoroff, L. B. Nguyen, E. Dogan, D. Rosenstock, C. Wang, K. N. Nesterov, M. G. Vavilov, and V. E. Manucharyan, (2021), arXiv:2103.04491 [quant-ph].

[18] G. Paraoanu, Physical Review B **74**, 140504 (2006).

[19] J. M. Chow, A. D. Córcoles, J. M. Gambetta, C. Rigetti, B. R. Johnson, J. A. Smolin, J. R. Rozen, G. A. Keefe, M. B. Rothwell, M. B. Ketchen, and M. Steffen, Phys. Rev. Lett. **107**, 080502 (2011).

[20] J. M. Epstein, A. W. Cross, E. Magesan, and J. M. Gambetta, Phys. Rev. A **89**, 062321 (2014).

[21] M. Carroll, S. Rosenblatt, P. Jurcevic, I. Lauer, and A. Kandala, "Dynamics of superconducting qubit relaxation times," (2021), arXiv:2105.15201 [quant-ph].

[22] N. Sundaresan, I. Lauer, E. Pritchett, E. Magesan, P. Jurcevic, and J. M. Gambetta, PRX Quantum **1**, 020318 (2020).

[23] A. W. Cross, L. S. Bishop, S. Sheldon, P. D. Nation, and J. M. Gambetta, Phys. Rev. A **100**, 032328 (2019).

[24] B. K. Mitchell, R. K. Naik, A. Morvan, A. Hashim, J. M. Kreikebaum, B. Marinelli, W. Lavrijsen, K. Nowrouzi, D. I. Santiago, and I. Siddiqi, Phys. Rev. Lett. **127**, 200502 (2021).

[25] J. M. Chow, L. DiCarlo, J. M. Gambetta, F. Motzoi, L. Frunzio, S. M. Girvin, and R. J. Schoelkopf, Phys. Rev. A **82**, 040305(R) (2010).

[26] D. C. McKay, C. J. Wood, S. Sheldon, J. M. Chow, and J. M. Gambetta, Phys. Rev. A **96**, 022330 (2017).

[27] S. Sheldon, E. Magesan, J. M. Chow, and J. M. Gambetta, Phys. Rev. A **93**, 060302 (2016).

[28] S. Sheldon, L. S. Bishop, E. Magesan, S. Filipp, J. M. Chow, and J. M. Gambetta, Phys. Rev. A **93**, 012301 (2016).

[29] E. Magesan, J. M. Gambetta, B. R. Johnson, C. A. Ryan, J. M. Chow, S. T. Merkel, M. P. da Silva, G. A. Keefe, M. B. Rothwell, T. A. Ohki, M. B. Ketchen, and M. Steffen, Phys. Rev. Lett. **109**, 080505 (2012).